

Article

Geomorphological Analysis of Xilokastro Fault, Central Gulf of Corinth, Greece

Sotirios Verroios and Vasiliki Zygouri *

Department of Geology, University of Patras, 26504 Rion, Greece; verroios@upatras.gr

* Correspondence: zygouri@upatras.gr

Abstract: The Gulf of Corinth is a rapidly opening area with high seismicity associated with extensive building collapses, destruction of cities, and even the deaths of inhabitants. Rapid residential development, especially in the southern part of the Gulf of Corinth, and the construction of crucial technical infrastructures necessitate understanding the activity across crustal-scale faults that host devastating earthquakes. The evolution of landforms affected by fault action is a dominant issue in geological science. In the present study, was selected the 20 km long Xilokastro pure normal fault. In this fault, we apply eight geomorphological indices in footwall catchments that drain perpendicular to its trace. In total, more than 5000 measurements were made in 102 catchments. The determination of geomorphological indices requires the construction of morphological profiles either perpendicular to the faults or perpendicular to the main tributaries of the drainage basins under consideration through the use of the geographical information systems (ArcGIS platform). The application of these indices along catchments draining the Xilokastro fault scarp show high active tectonics. Its high activity is evidenced by the high values of the length-slope index near the fault trace, the low values of the width to height ratio index, the strong asymmetry of the drainage basins, especially in the overlapping zones between its segments, and the elongated shape of the drainage basins. This study supports the idea that the application of a single morphometric index is unable to reflect the distribution of active tectonics across faults, which makes inevitable the systematic comparison of a series of tectonic morphometric indices from which a new combined index emerges (Iat). The Iat classifies the Xilokastro fault in the high degree of activity at a rate of 75% of its length.

Keywords: morphogenic faults; geomorphic indices; Xilokastro fault; Gulf of Corinth



Citation: Verroios, S.; Zygouri, V. Geomorphological Analysis of Xilokastro Fault, Central Gulf of Corinth, Greece. *Geosciences* **2021**, *11*, 516. <https://doi.org/10.3390/geosciences11120516>

Academic Editors: Olivier Lacombe and Jesus Martinez-Frias

Received: 20 November 2021

Accepted: 13 December 2021

Published: 16 December 2021

Publisher's Note: MDPI stays neutral with regard to jurisdictional claims in published maps and institutional affiliations.



Copyright: © 2021 by the authors. Licensee MDPI, Basel, Switzerland. This article is an open access article distributed under the terms and conditions of the Creative Commons Attribution (CC BY) license (<https://creativecommons.org/licenses/by/4.0/>).

1. Introduction

The evolution of tectonically controlled landforms and the way active tectonics of an area are imprinted has caused a great deal of research by and discussion among the scientific community [1]. Understanding the geometry of faults, the interaction between faults, and the sensitivity of river systems to tectonic movements becomes extremely important in determining the active tectonics of an area [2–6]. Therefore, its associated hazards, such as tectonic movements, liquefactions, and floods can be predicted as well. Fault growth, whether achieved by the joining of smaller cracks or by radial widening of a pre-existing fault, is a process with numerous stages of development, most of which cannot be detected. However, the use of geomorphological methods in areas of active tectonics, which are associated to strong seismicity, leads to conclusions and quantifies the changes in the terrain along a fault, and it can be an indication of the slip rate in an active fault.

The Gulf of Corinth (Figure 1) is a basin with the fastest extension rate in Europe [7–9]. The existence of many faults of normal geometry in its southern margin is “responsible” for the impressive topography in the gulf [10–12]. Deltaic sediments, which are currently uplifted, located on the footwall of normal faults, imply the continuous supply of the bay with sediments. The intense tectonic activity ensures conditions required for capturing tectonic movements in landforms. By this way the landforms become “able” to provide data on the tectonic evolution of an area for both short-term and long-term observation periods.

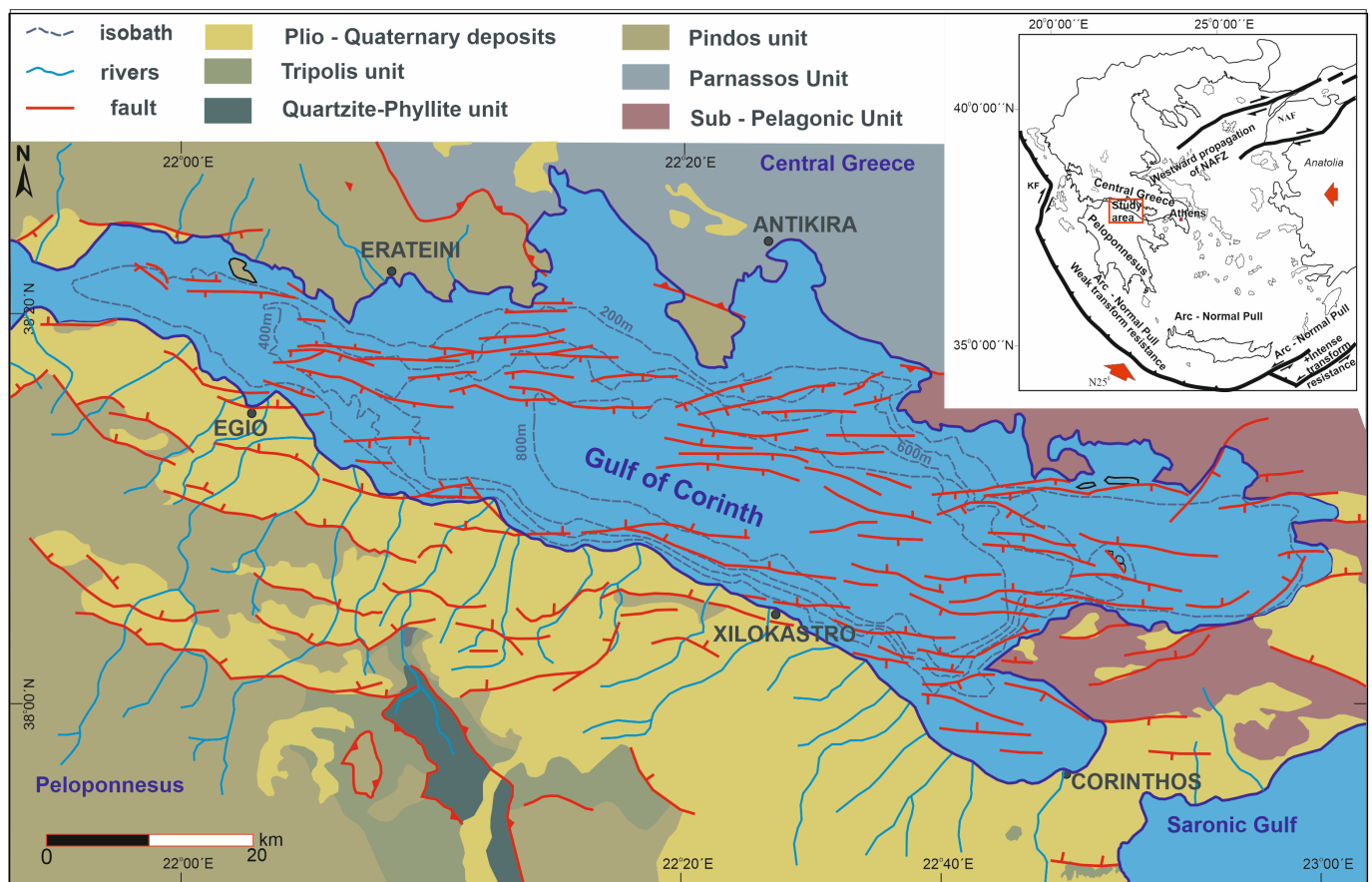


Figure 1. Simplified map of the Gulf of Corinth (modified by [13,14]). The inset figure shows the geological setting of the study area.

Extensive research has been conducted in the Gulf of Corinth in recent decades, covering different geological activities (e.g., [13,15–20]). Active faults in the southern margin of the Gulf of Corinth causes a combination of movements that vary from west to east [19,21]. This combination of movements consists of N-S maximum extension of 16 mm/yr and increasing elevation towards the west [19,22–24], reaching 1.85 mm/yr in the southwest margin [25] as is expressed by the occurrence of strong seismic events in the area [26–32]. The intense tectonic activity, which is concentrated mainly in the southern part of the bay, results in the creation of a high relief in the area. The stratigraphy of the Gulf consists mainly of geological formations of the Mesozoic that belong to the units of Olonos—Pindos, Tripoli, and Sub-Pelagonic. The orogenic processes began in the Eocene [33], resulting in the creation of the Greek orogenic belt. During the final stages of orogeny, during the Neogene, several processes began, such as the formation of river basins, the accumulation of sedimentary deposits such as clays and conglomerates that gradually turn into marls [16,34–39], and submarine fans in the bottom of the Gulf [40–43]. In addition, fault activity in the southern margin of the basin raised these deposits more than 400 m above sea level, forming a succession of marine terraces that are quite extensive in the southeastern part of the Gulf [15,16,44–46]. The evolution of the Gulf highlights a dynamic process that changes over time [47–49]. The majority of researchers distinguish two stages of development. At first the Gulf formed a shallow basin where terrestrial sediments were deposited, while gradually in the second stage the Gulf achieved its current geometry by developing delta ridges within the Gulf of Corinth depocentres [13,15–18,50–52]. However, [53] and later [45] claim that during glacial periods the sea level decreased, resulting in the isolation of the bay and the change of sedimentation rates. The tectonic-stratigraphic evolution of the Gulf of Corinth represents the complexity of the processes found in other rift basins

such as the Gulf of Suez, and for this reason despite the abundance of research work the Gulf of Corinth continues to attract the interest of geoscientists despite its age as relatively new (< 5 million years) compared to other rifts.

Tectonic geomorphology is a relatively new tool at the disposal of geoscientists, which, although initially showing only qualitative estimates, the use of innovative observation instruments gave accurate observations and the necessary quantification for modern society. It serves multiple temporal and spatial scales by examining how the horizontal and vertical deformation of the earth surface can affect the shape of hills or streams in an effort to better understand the distribution of stresses along active faults [2,6,54,55]. In Greece, systematic research in the field of tectonic geomorphology is rather limited [56–59], and the river network response associated with high tectonic activity is poorly understood [60–63]. Therefore, the question arises whether landforms that are subject to the action of both external and internal processes can evidence tectonic activity and describe the fault evolution (Figure 1). In addition, the Gulf of Corinth, showing a dense network of active normal faults that host a large number of landforms, constitutes a prominent study area as it is rather easily assessable and the structures are newly formed and thus not eroded.

The aim of this study is the detailed geomorphological analysis of the evolution of landforms in the area of Xilokastro fault, located in the central part of the Gulf of Corinth. The Xilokastro fault dominates the seismic activity of the Corinthian and is representative example of morphogenic fault associated with high slip rates. Its morphology and geometry are analyzed using geomorphic indices that indicate the influence of active tectonics in river drainage orientation and sediment distribution.

2. Geological Setting

Detailed tectonostratigraphy studies show that extensional basins are not simple geometrical structures, but evolve over time. Observations of geometry as well as the evolution of the structure of an extensional basin provide important information on large-scale lithospheric processes and the mechanical properties of faults. Despite their scientific, social, and economic significance, understanding of how extension begins and how it progresses remains limited mainly due to the few examples of active extensional basins. These are the Red Sea or the Gulf of Aden. A typical example of active extension in Europe is the Gulf of Corinth, which is an extremely new structure with a large volume of sediments and, at the same time, high seismicity rates. The Gulf of Corinth with a general orientation WNW-ESE separates the Peloponnese from central mainland Greece (Figure 1). Geodetic extension over the last 20 years shows an increase from 6 mm/yr in the east to 16 mm/yr in the west [7,24,31].

The northward movement of the African plate results in its subsidence below the Eurasian plate, with a convergence rate of 1 cm/yr [47]. The movement of the Arabian plate to the north has caused compression around the Black Sea [64], resulting in a western extrusion of Turkey in relation to the Eurasian plate. This movement is currently taking place along the dextral transfer fault of the North Anatolia, and leads gradually to the southwest movement of the East and Aegean microplate, relative to the Eurasian plate [65,66]. The modern convergence with NE-SW direction was measured to be achieved at rates of 3–5 cm/yr in the Hellenic arc ([23]; Figure 1 inset). In addition, micro-seismic studies [67] and geophysical seismic wave tomographies [68], in an attempt to trace the subsidence of the African plate, showed that the subduction angle changes gradually from mild to abrupt subsidence below the Gulf. The Gulf of Corinth is regarded to be the most active graben within the Aegean microplate (Figure 2) between the SW end of the North Anatolian fault and the dextral strike slip fault of Kefalonia [8,69,70]. It extends more than 100 km in WNW—ESE direction [19,34] while it grows at an angle in relation to the NNW extending Hellenides (Figures 1 and 2), occupying a maximum width of 30 km.

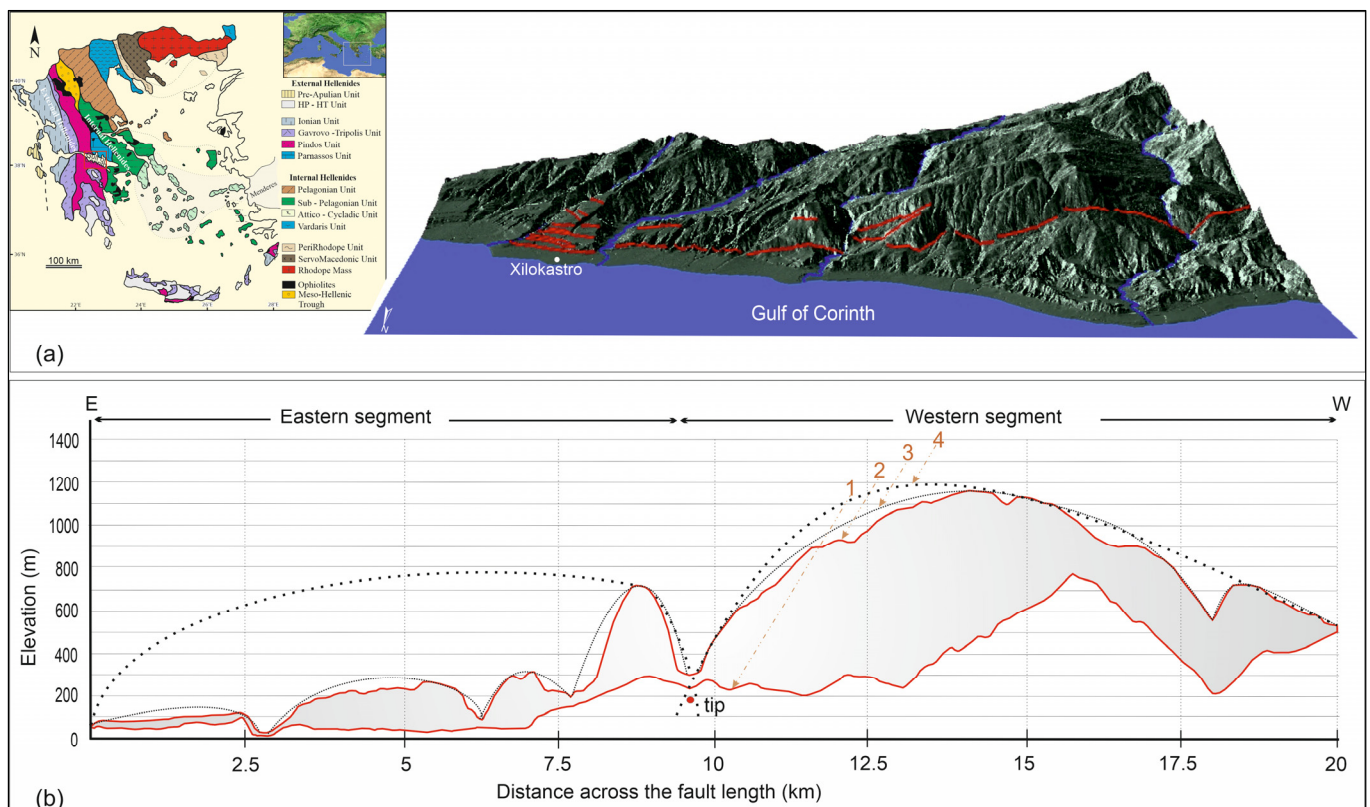


Figure 2. (inset) Geological setting of Greek peninsula; (a) 3D model of the Xilokastro fault constructed through the ArcScene platform. The red line is the trace of the rift as mapped during field work. (b) Topographic profile of the displacement of the hanging wall (line 1) and the footwall (line 2) of the fault. Line 3 illustrates the normalized topography of the individual ruptures along the fault section, and line 4 illustrates the overall topographic representation of the two main sections of the fault.

The geomorphological structure between Corinth and Xilokastro is characterized as relatively mild as it forms rivers and marine terraces [16]. In this area there are no densely ruptured slopes resulting in the mild morphology of the relief [8,16,21]. These terraces cover a large area and are limited to the west by the impressive ruptured slope formed by the action of the Xilokastro fault. Its trace is located in the area southwest of the coastal city of Xilokastro. Its length reaches almost 20 km but its most impressive slope is set at 11.6 km, where in this area the fault scarp is impressive and is estimated at 0.8–1 km (Figure 2a). It is characterized by normal sense of movement in an almost W-E orientation, dipping to the north. It is composed of an onshore and an offshore part [71,72]. The offshore part, which does not exceed 6 km in length, shows, according to underwater geophysical surveys, a slope height of 580 m ([50]; Figure 2b) and is related to the deposition of modern turbidites towards the centre of the trench of The Gulf of Corinth that come from high sediment supply of rivers draining the area east of Xilokastro [71]. Its onshore part is not uniform but shows high segmentation (Figure 2b). According to [73], the Xilokastro fault is probably the boundary between the deformation that diffuses into several faults in the western part of the Gulf of Corinth and the eastern one in which the deformation is now hosted in a small number of faults that are mainly located within the offshore part of the gulf. The main phase of its activity is occurred approximately 1.5–0.7 million years ago [20,52]. Its surface trace based on extensive field work showed the existence of segments with length 500–2500 m. The western end of the fault shows larger sections of faults than the eastern one. In addition, its topographic detection (Figure 2b) decreases dramatically at the eastern end of the fault. The value of maximum topographic elevation reaches 1180 m, while the separation between the eastern and western part is evident, accompanied by a corresponding reduction in displacement. The Fonissa River flows in

between the two prominent segments of the fault (Figures 2 and 3). The maximum visible displacement along the fault is approximately 900 m and is located in the western part (Figure 2b). The fault footwall consists of Mesozoic limestones [74,75] in its western part, whereas in the eastern part there are elevated marine terraces (Figure 3). Surface scarps appear in the western part of the fault (Figure 3b,c,e). Curvatures are identified on these surfaces, whereas slip lines are compatible with the normal sense of motion of the fault (stereographic projections in Figure 3). The footwall of the fault is bounded by colluvial deposits that include clay formations with scattered conglomerates (Figure 3f,g). Towards the east, in its footwall Pleistocene marls and conglomerates are exposed (Figure 3h).

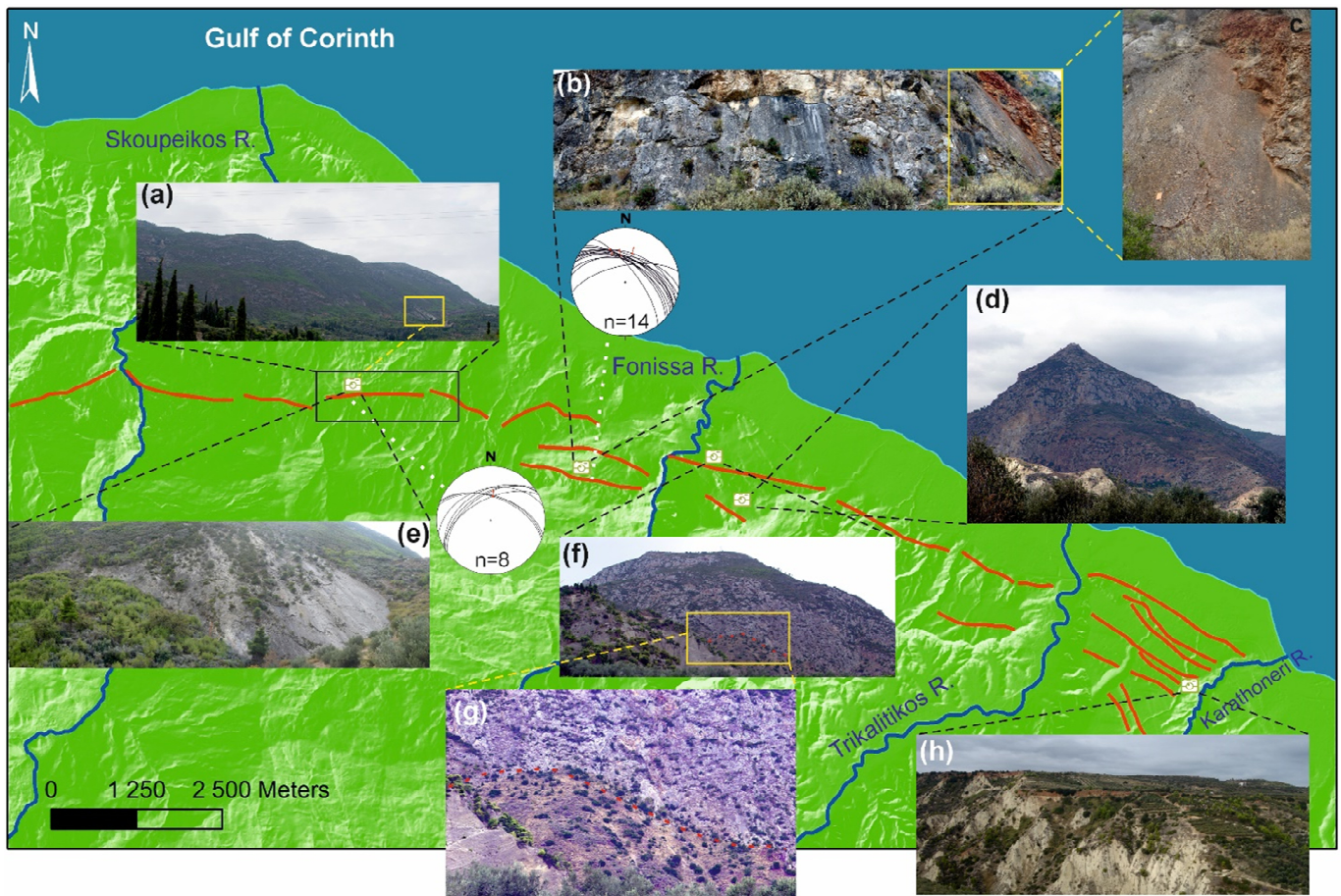


Figure 3. Simplified map of the Xilokastro fault showing stereographic projections of the polished surfaces and the sliding lines of the main scarps whose position is marked with a white dashed line. In addition, photos taken during field work are displayed, the locations of which are symbolized by the image of the camera. The yellow box marks parts of the photos that are presented in a larger scale. (a) Panoramic view of the western part of the Xilokastro fault (its exact location is marked with a black box on the map). (b) Photomosaic of the scarp derived that appears on Ano Loutro–Kato Loutro road. (c) Detail view of the same surface. (d) Panoramic view of the eastern part of the fault. The hill is known as “Panagia Korifis”. (e) Photomosaic of a fault surface marked in the yellow frame of the photo in (a). (f) Colluvial deposits accumulating at the base of the fault. (g) Detailed geometry of the background with the Neogene formations. (h) Successive sea terraces at the eastern end of the fault.

3. Materials and Methods

Geomorphological indices have been used systematically to evaluate active tectonic structures in various parts of the world ([58] and references therein). The structures primarily used in the geomorphological analysis are the active slopes, the river basins, and the drainage networks. Internal tectonic processes deform the Earth’s surface, whereas external processes shape the final morphological expression. Any disturbance caused by

these processes alters the dynamic equilibrium of the system, which can be observed in the properties of river networks that drain tectonically active slopes [6,76,77]. In particular, river basins represent dynamic systems that can provide evidence of the formation and evolution of a tectonic structure [78,79]. The numerical representation of the topographic features is implemented through mathematical relations that can be divided into two sections (spatial and tectonic geomorphological indices), depending on the parameters of each index [80–83].

Across the orientation of the Xilokastro fault, 102 catchments were identified that dissect the fault almost perpendicularly. The main morphotectonic indices were calculated (Table 1). The runoff direction of each basin is considered to be the same as the general N-S orientation of the extension. However, there is a change in the lithology that is eroded between the eastern and western part of the fault, whereas the effect of climate is considered similar along the entire fault. The drainage network is characterized from parallel to sub-parallel, attributing its formation mainly to the fault evolution. The catchments show a variety of sizes and shapes (Figure 4). The fault is also drained from the four major catchments of the rivers Skoupeikos, Fonissa, Trikalitikos, and Katharoneri of general direction N-S whose runoff has also been affected by the action of the Xilokastro fault according to [37], forming wind and water gaps in the past.

Table 1. Main morphometric indices calculated for the drainage basins along the Xilokastro fault front.

Geomorphic Indices	Mathematical Formula	Xilokastro Fault
		Number of Calculations for Each Index
Number of valleys		102
Drainage basin shape B_s ^(1, 2)	$B_s = B_L/B_w$	102
Elongation Basin Index R_L ^(1, 2)	$R_L = 2\sqrt{(A/\pi)}/L$	102
Circularity Basin Index R_c ^(1, 2)	$R_c = 4\pi A/P^2$	102
Asymmetry Factor AF ^(1, 3)	$AF = 100(A_r/A_t)$	102
Transverse Topographic Symmetry Factor T ^(1, 3)	$T = D_a/D_d$	881
Stream length-gradient index SL ^(1, 4)	$SL = (\Delta_H/\Delta_L)L$	845
Valley Floor Width–Valley Height Ratio V_f ^(1, 5)	$V_f = 2V_{fw}/[(E_{ld} - E_{sc}) + (E_{rd} - E_{sc})]$	1673
Hypsometric integral Hi ^(1, 6)	$Hi = (h_{mid} - h_{min})/(h_{max} - h_{min})$	1859

(1) = For the definition and calculation of the geomorphic indices described in the current analysis see [58,59,84] and references therein. (2) = Elongated catchments (tectonically active) usually have a small secondary network compared to circular catchments (inactive tectonics), which have a network with branches of many orders [85]. (3) = The development of a river basin network in stable geological conditions results in absolute symmetry for basin and river characteristics. Any tectonic force affects this ideal symmetry [86]. (4) = When the elongated profile of a riverbed differs from the typical profile, then the differentiation reveals changes in the lithology and the tectonics of the area [87]. (5) = Streams with a narrow riverbed and steep banks show V-shaped river valleys characterized by deep erosion, whereas a wide riverbed with gentle banks forms a U-shaped river valley showing the prevail of erosion against tectonic forcing [88]. (6) = The Hypsometric Integral index marks the stage of evolution in which the catchment is in relation to the erosion cycle [1,69].

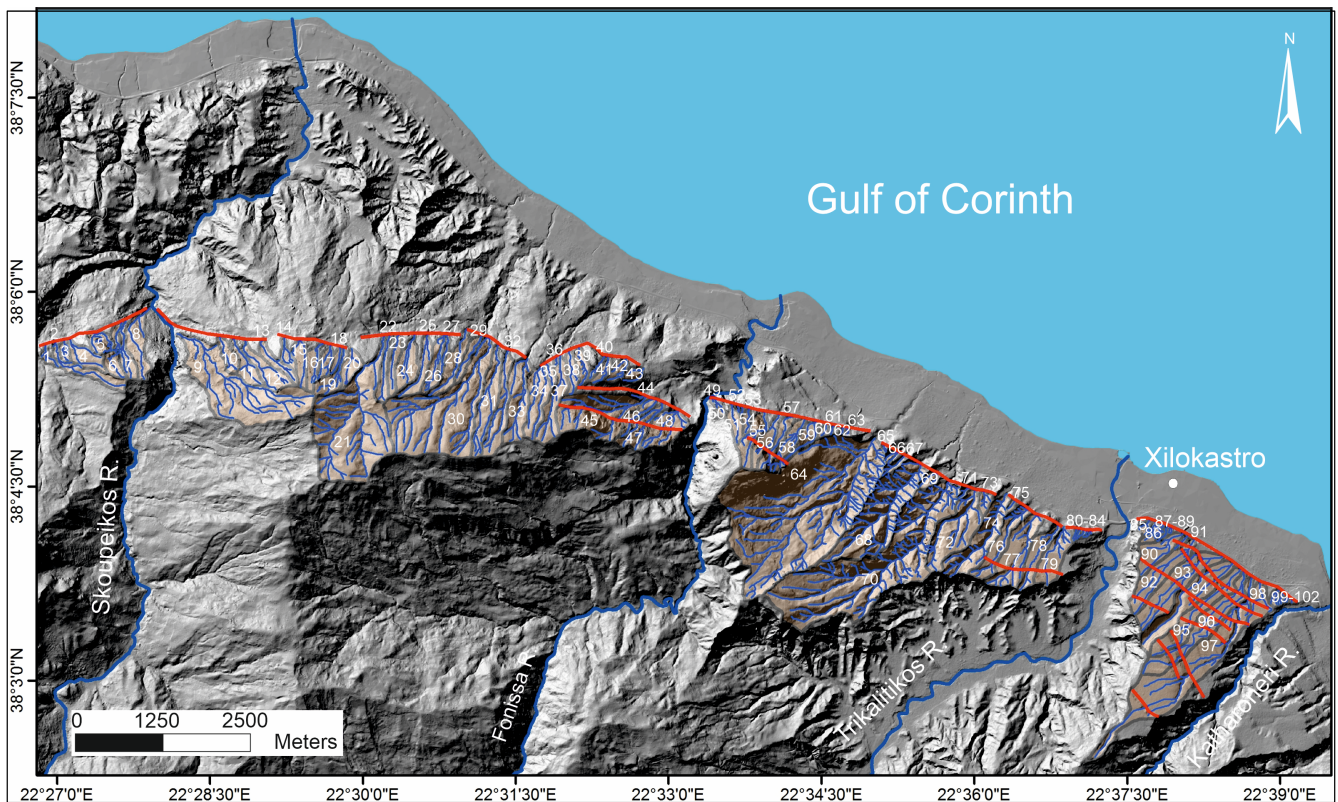


Figure 4. A 3D relief model of the hydrographic network that develops along the orientation of the Xilokastro fault. The catchments highlighted in bright pink intersect its trace and are numbered from the west to the east end of the fault.

4. Results

We examined the spatial distribution of the catchment shape factor B_s based on the calculation of the length to the width of the catchment and not its surface. The catchments can be separated in more detail, into very long ones that have values higher than 4 and are connected to high percentages of active tectonics. A second class of basins are classified as elongated with values in the interval 3–4, which indicate active tectonics, and others that are less elongated and have values lower than 3. These less elongated basins are characterized by lower active tectonics. According to this classification of [89], approximately 60% of the catchments along the Xilokastro fault (Figure 5a) show evidence of active tectonics based on their shape, which in most of them is characterized as elongated. In addition, both the catchment area elongation index R_L and the circularity index of the catchment area R_C prove that almost all the basins along the Xilokastro fault can be characterized as elongated to very elongated (Figure 5b,c). Therefore, the drainage of the fault footwall is mainly formed from the main branches of the basins by direct discharge of the secondary branches to the main branches, which will show high erosion capacity.

The AF catchment asymmetry index calculated at 102 catchments along the Xilokastro fault indicates a wide range of values, and for this reason its values were grouped at specified numerical intervals (Figure 6a). The classification of [89] regards values between 45 and 55 that do not show any preferred slope and are considered to grow in stable geological conditions. Values above or below this range indicate basin asymmetry either to the west (values > 55) or to the east (values < 45). Along the Xilokastro fault, the catchments are mostly considered asymmetric (Figure 6a) without, however, a uniform general tendency, a fact that is probably related to the fault segmentation. However, there are sub-trends that highlight a westward turn of the catchments located in the western part of the fault, which become even stronger towards its western boundary and obviously affects the catchments just east of Skoupeikos that are tilted to the east. Exactly the same

phenomenon is observed at the natural border between the western and eastern part of the fault, Fonissa.

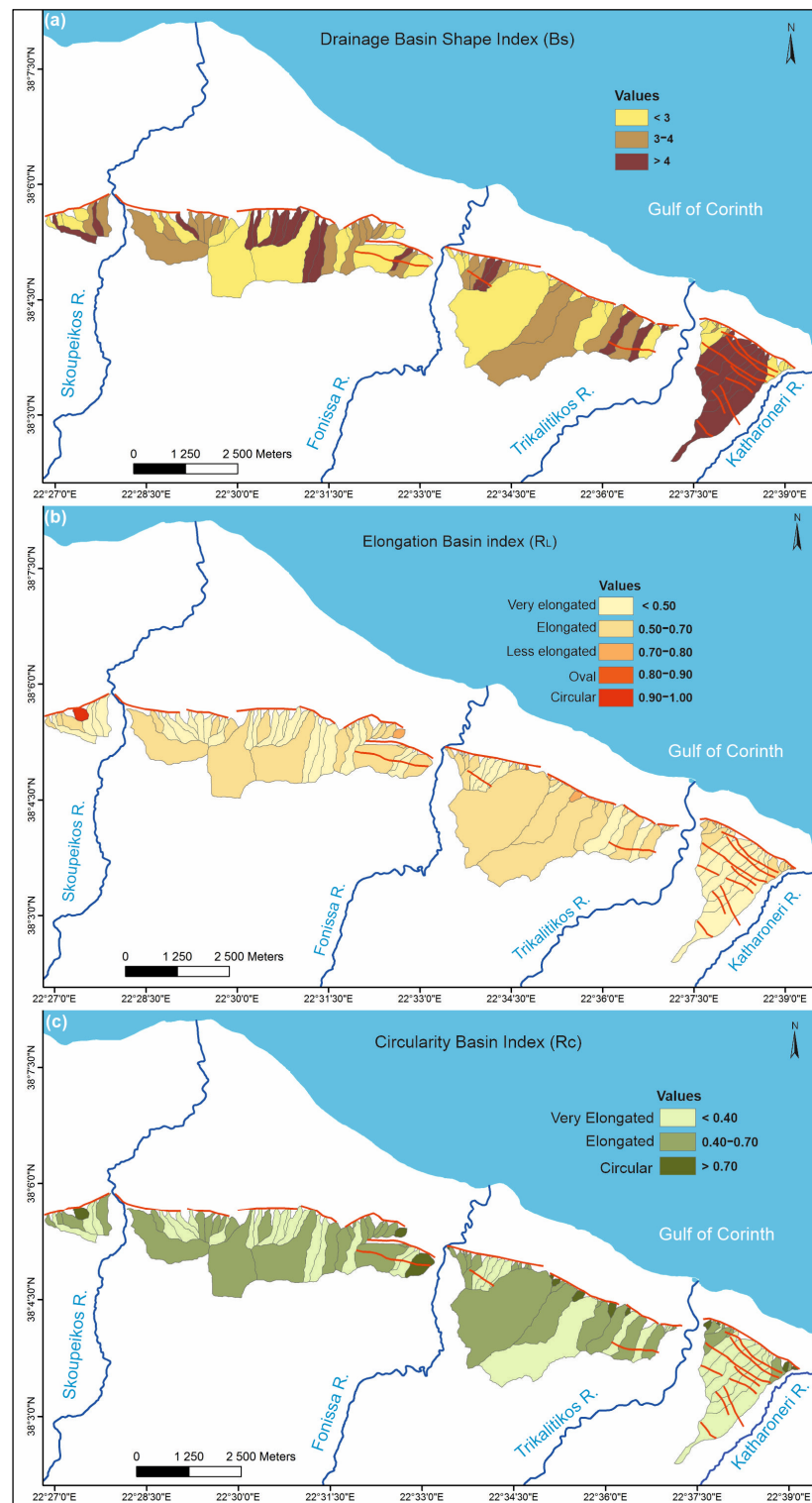


Figure 5. (a) Spatial distribution of the drainage basin index Bs. The red line symbolizes the trace of the Xilokastro fault. Smaller sedimentary faults in the area have been projected between the rivers Trikalitikos and Katharoneri. (b) Spatial distribution of the RL elongation basin index. (c) Spatial distribution of the RC circularity basin index.

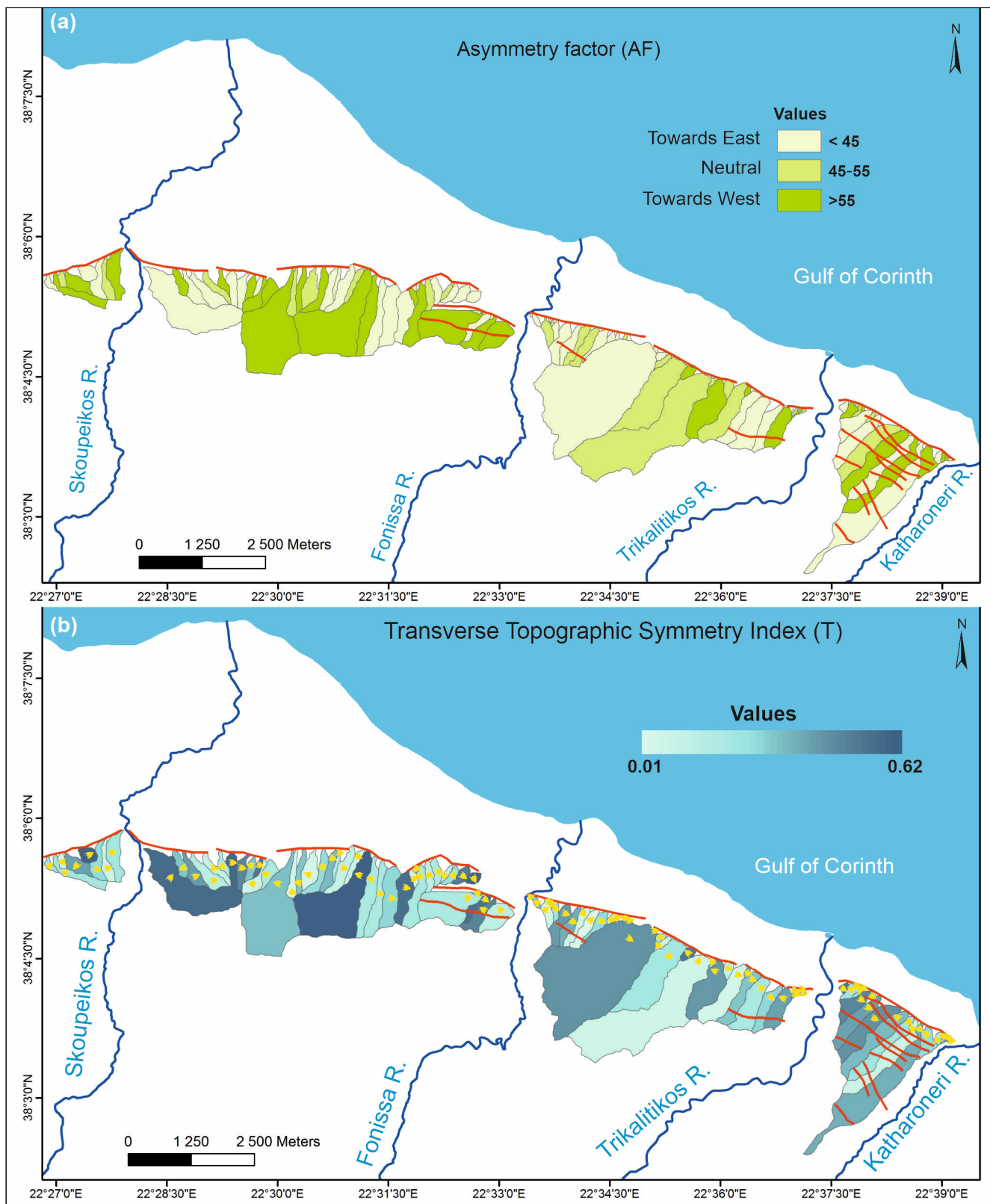


Figure 6. (a) Spatial distribution of the AF basin asymmetry index. (b) Spatial distribution of the transverse topographic index T. The colours in the catchments along the fault correspond to the average size calculated for each basin and the yellow arrows in the middle show displacement direction of the main branch of each basin.

Therefore, both areas around the river systems of Fonissa and Skoupeikos are affected by the fault's activity. The analysis of the transverse topographic symmetry index T for all catchments along the Xilokastro fault includes the calculation of a vector that has size and orientation. The spatial distribution of these values is shown in Figure 6b, which also shows the orientation of the mean vector with a yellow arrow. As can be seen, the individual trends shown by the AF basin asymmetry index are also confirmed by the orientation of the mean vectors determined for the transverse topographic symmetry index T (Figure 6b). A characteristic example is the area around the Skoupeikos River, where strong values of asymmetric slope according to the asymmetry index AF and similar orientation of the mean vector of the index of transverse topographic symmetry T (Figure 6).

For the SL length-slope index, a density map was constructed with the aim of distinguishing the areas of the basins that show higher values of the index and therefore correspond to areas of high anomaly from the ideal elongated topographic profile of the riverbed. Areas of high anomaly in the index values are associated with high tectonic activity. According to the map of Figure 7a, the areas of high anomaly and therefore of high tectonic activity are located in the western part of the fault, mainly along its trail. Respectively, in the eastern part of the fault in the area between Fonissa and Trikalitikos there are no correspondingly high irregularities except for the fault trace that is located very close to Fonissa and showed signs of high tectonic activity and the asymmetry indices of the basin topographic symmetry T . In addition, the distribution of the high values of the index in the area near Katharoneri should be noted, in which smaller ruptured structures are observed. A corresponding density map was constructed for the values of the ratio valley floor to valley height V_f . Index values are grouped into three classes [80,84,88,90,91]. This grouping correlates the index values with active tectonics classes. In this way, high values of the index (>1) correspond to low active tectonics, whereas low values of the index (<0.5) indicate high uplift rates. According to this separation and the measurements in the present analysis, the majority of the values of the geomorphic indices along the Xilokastro fault fall within the field of high uplift rates at the footwall of the fault (Figure 7). However, it seems that the lithology also plays a very important role as the largest cluster of low values is located in the area between Fonissa and Trikalitikos in the eastern part of the fault (Figure 7). The small size of these values is related to lithology, as in this area the streams flow in deltaic deposits forming high deep erosion and therefore relatively small widths in the active riverbed. However, a general observation that is easily deduced is that low values of the index are observed almost along the entire length of the fault trace.

Finally, for the Hypsometric integral index as shown in Figure 7c, it is striking that several basins in the western part of the fault are in a young stage. The remaining basins along the fault are placed in a mature stage, with only three basins being in an aged stage. The catchments classified in an aged stage are located in both parts of the fault. They are characterized by their size, which is impressive. One of them is the largest basin, which, as shown in Figure 7c, is less elongated and therefore is expected to be classified as old. However, the same basin exhibits low values of valley floor to width ratio due to its lithology. The other two basins are extremely small in size, which would be expected to be associated with earlier stages of erosion. Probably, their classification in the old stage is due to the "effort" of the catchments to increase their hydrodynamic capacity by attracting adjacent basins or to be a non-ruptured point in the fault (persistent segment barrier).

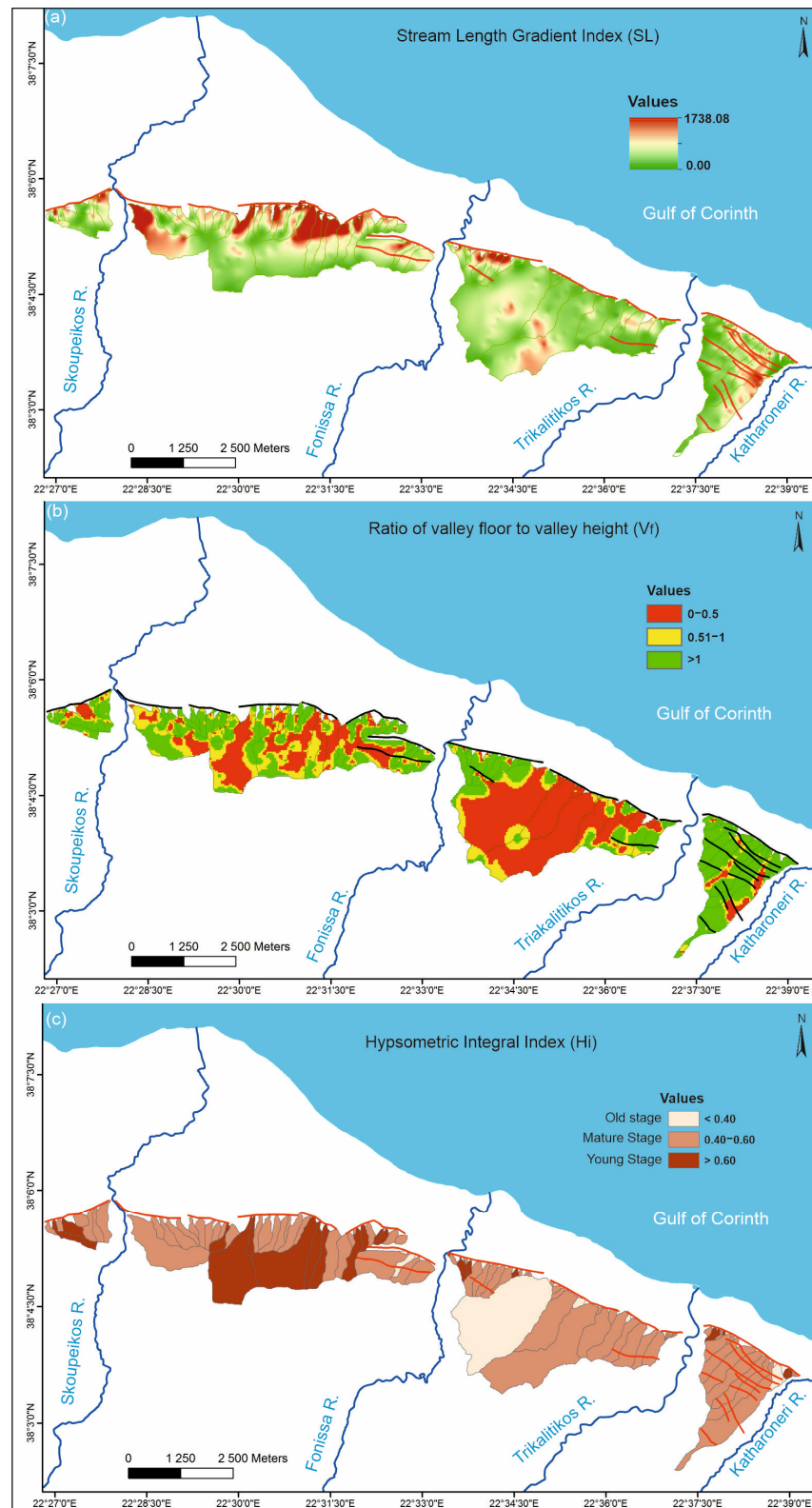


Figure 7. (a) Spatial distribution of SL length-slope value values. The green to yellow areas indicate areas where the values of the index show from no to small anomaly, whereas the red areas indicate the areas that are dominated by very high anomalies. (b) Spatial distribution of values of the ratio of valley floor to valley height Vf. The red areas correspond to high tectonic activity, whereas the yellow areas indicate the moderate tectonic activity sites, and the green areas highlight low tectonic activity areas. (c) Spatial distribution of the hypsometric integral Hi.

5. Discussion

For the overall assessment of the active tectonics in the whole area of the Xilokastro fault, the geomorphological indices were joined in a combined index *Iat*. These are the basin-shaped coefficient indices of the catchment area *Bs* and the tectonic morphometric indicators except the index of the transverse topographic symmetry *T*. The index distribution identifies the most active sections of the fault via ArcGIS by presenting a rather simplified map of tectonic activity along the fault (Figure 8). Based on the distribution of the combined index *Iat*, its values that are less than 2 represent high tectonic activity. Areas with high tectonic activity occur in both the western and eastern part of the fault, although the steepest slopes in the topographic profile are observed in the west. However, both the findings from the SL stream length-slope index for the western part and those of the valley floor-to-height ratio for the eastern part are compatible with the distribution of the combined index. In addition, special note should be made of the areas that flow through the rivers Skoupeikos, Fonissa, Trikalitikos, and Katharoneri. Except for the area of Skoupeikos, where high tectonic activity occurs in other areas, the active tectonics is clearly lower. Considering the AF basin asymmetry index, the creation of an overlap zone is evident, especially in the area of Fonissa, and is also seen in the Skoupeikos area. As for the eastern and western boundary of the fault, they seem to disappear in the area and therefore the results of the geomorphological analysis do not support either the merging with the submarine part of the fault to the east or the westward propagation of the fault. Similar observations were made for the Xilokastro submarine fault by [41,50] and for the western part of Xilokastro and its possible merge with the Valimi fault by [20,52].

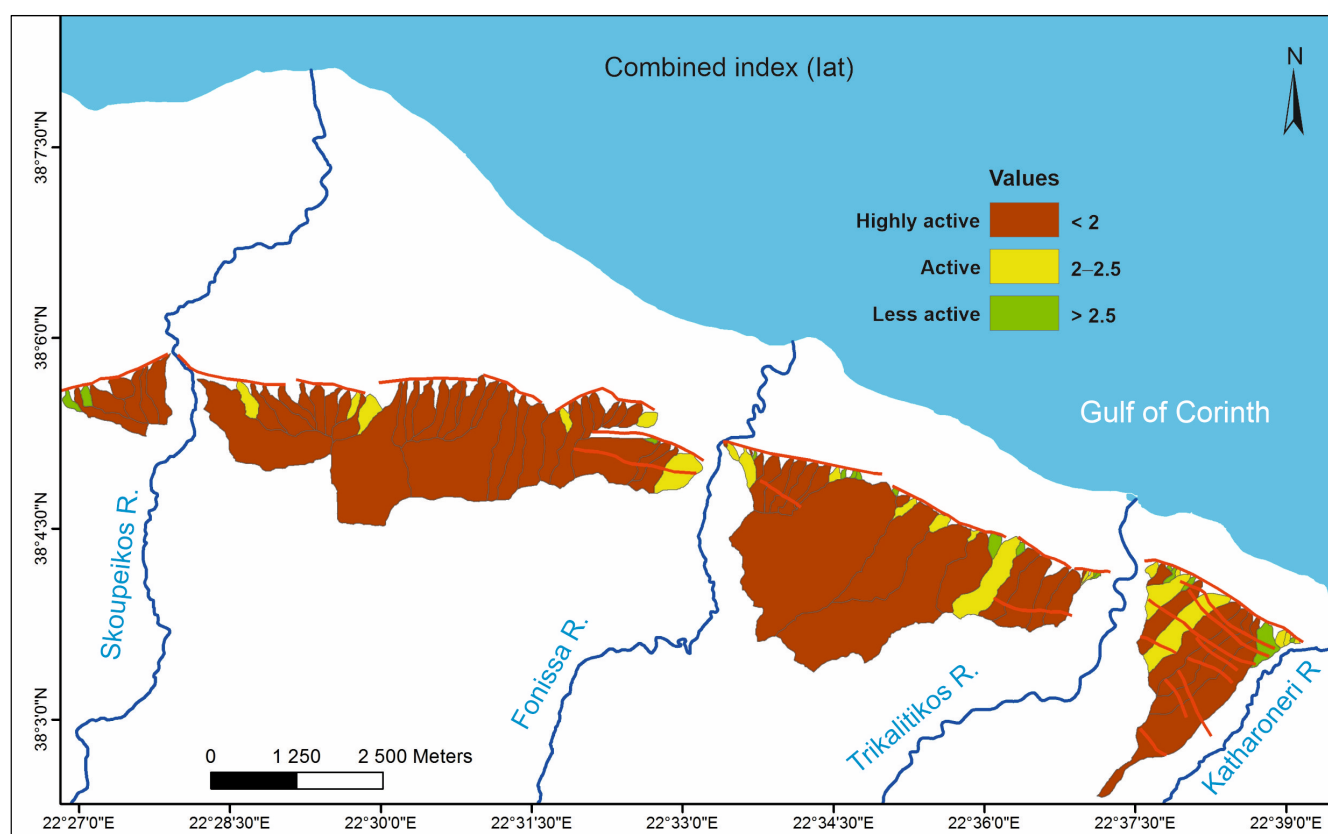


Figure 8. Spatial distribution of the combined index *Iat*.

Based on the combined index (*Iat*) (Figure 8) that resulted from the detailed morpho-tectonic analysis of Xilokastro fault, the fault slip rate was calculated. According to [92] the slip rate at highly active fault scarps corresponds to 0.08 mm/yr, whereas according to [93], it was found to be 0.4–0.5 mm/yr. The distribution of the combined index showed

that along the Xilokastro fault the largest percentage of runoffs belongs to the order of highly active tectonics (Figure 8) with almost straight foothills, main runoff channels of deep erosion, elongated runoff basins, and changes in the topographic profiles of the streams that develop at the fault footwall. All these results derived from the morphotectonic analysis of the faults demonstrate rapid rates of vertical erosion and tectonic slip. In addition, the data are compatible with the morphometric analysis of [94], who applied morphometric measurements across ten pre-existing river systems along the south coast of the Gulf of Corinth.

6. Conclusions

The variability in the distribution of the values of the geomorphological indices significantly influences the classification of the whole fault and its segments into classes of tectonic activity. The application of geomorphological indices seems to be extremely useful in areas that are not dominated by very high activity that, although they have clear evidence of tectonic activity—such as the Xilokastro fault, with its impressive fault scarp—do not record recent incidents of seismic activity. The conclusions from the present study are:

- The application of the geomorphological indices along 102 small basins along the Xilokastro fault proposes high fault activity.
- Although the fault shows high activity, the prominent segment linkage is not achieved. These segments are defined by the Skoupeikos, Fonissa, and Trikalitikos antecedent rivers.
- Its high degree of tectonic activity is certified by the high values of the length-slope index near its trace, by the low values of the valley floor-to-height ratio index, the strong asymmetry of the catchments, especially in between overlapping segments, and from the elongated shape of its catchments.
- Its morphotectonic impact according to the index of hypsometric integral is in a young stage, especially in the western part of the fault, which shows the steepest relief, but no signs of fault propagation are recognized either to the west or to the east.

Therefore, for active faults whose paleoseismological history is unknown, morphotectonic analysis can help estimate key variables such as slip rate and recurrence time interval that are considered important elements for a seismic hazard analysis across a fault. Moreover, considering the possibilities provided by modern technology and the easily and economically feasible access to high-precision digital products, it seems that geomorphological indices contribute to the determination of fault activity.

Author Contributions: Conceptualization, S.V.; methodology, S.V. and V.Z.; software, S.V.; validation, S.V.; formal analysis, S.V. and V.Z.; investigation, S.V.; resources, S.V.; data curation, S.V.; writing—original draft preparation, S.V. and V.Z.; writing—review and editing, S.V. and V.Z.; visualization, S.V. and V.Z.; supervision, V.Z.; project administration, S.V. and V.Z. All authors have read and agreed to the published version of the manuscript.

Funding: This research received no external funding.

Institutional Review Board Statement: Not applicable.

Informed Consent Statement: Not applicable.

Data Availability Statement: Not applicable.

Acknowledgments: The authors are grateful to the referees for their constructive and positive comments and to all editors for the excellent managing and suggestions on the manuscript.

Conflicts of Interest: The authors declare no conflict of interest.

References

1. Keller, E.A.; Pinter, N. *Active Tectonics: Earthquakes, Uplift and Landscape*, 2nd ed.; Prentice Hall: Hoboken, NJ, USA, 2002.
2. Whipple, K.X.; Tucker, G. Dynamics of the stream-power river incision model: Implications for height limits of mountain ranges, landscape response timescales, and research needs. *J. Geophys. Res. Space Phys.* **1999**, *104*, 17661–17674. [[CrossRef](#)]
3. Whipple, K.X.; Tucker, G.E. Implications of sediment-flux-dependent river incision models for landscape evolution. *J. Geophys. Res.* **2002**, *107*, 2039. [[CrossRef](#)]
4. Snyder, N.P.; Whipple, K.X.; Tucker, G.E.; Merritts, D.J. Landscape response to tectonic forcing: DEM analysis of stream profiles in the Mendocino triple junction region, northern California. *Geol. Soc. Am. Bull.* **2000**, *112*, 1250–1263.
5. Kirby, E.; Whipple, K. Quantifying differential rock-uplift rates via stream profile analysis. *Geology* **2001**, *29*, 415–418. [[CrossRef](#)]
6. Burbank, D.W.; Anderson, R.S. *Tectonic Geomorphology*, 2nd ed.; Wiley-Blackwell: New York, NY, USA, 2012.
7. Clarke, P.J.; Davies, R.R.; England, P.C.; Parsons, B.; Billiris, H.; Paradissis, D.; Veis, G.; Cross, P.A.; Denys, P.H.; Ashkenazi, V.; et al. Crustal strain in central Greece from repeated GPS measurements in the interval 1989–1997. *Geophys. J. Int.* **1998**, *135*, 195–214. [[CrossRef](#)]
8. Westaway, R. The Quaternary evolution of the Gulf of Corinth, central Greece: Coupling between surface processes and flow in the lower continental crust. *Tectonophysics* **2002**, *348*, 269–318. [[CrossRef](#)]
9. Avallone, A.; Briole, P.; Agatza-Balodimou, A.M.; Billiris, H.; Charade, O.; Mitsakaki, C.; Necessian, A.; Papazissi, K.; Paradissis, D.; Veis, G. Analysis of eleven years of deformation measured by GPS in the Corinth Rift Laboratory area. *Comptes Rendus Geosci.* **2004**, *336*, 301–311. [[CrossRef](#)]
10. Micarelli, L.; Moretti, I.; Daniel, J.M. Structural properties of rift-related normal faults: The case study of the Gulf of Corinth, Greece. *J. Geodyn.* **2003**, *36*, 275–303. [[CrossRef](#)]
11. Ghisetti, F.; Vezzani, L. Inherited structural controls on normal fault architecture in the Gulf of Corinth (Greece). *Tectonics* **2005**, *24*, 4016. [[CrossRef](#)]
12. Fernández-Blanco, D.; De Gelder, G.; Lacassin, R.; Armijo, R. Geometry of Flexural Uplift by Continental Rifting in Corinth, Greece. *Tectonics* **2020**, *39*, e2019TC005685. [[CrossRef](#)]
13. Bell, R.E.; McNeill, L.C.; Bull, J.M.; Henstock, T. Evolution of the offshore western Gulf of Corinth. *GSA Bull.* **2008**, *120*, 156–178. [[CrossRef](#)]
14. Zygouri, V.; Verroios, S.; Kokkalas, S.; Xypolias, P.; Koukouvelas, I. Scaling properties within the Gulf of Corinth, Greece; comparison between offshore and onshore active faults. *Tectonophysics* **2008**, *453*, 193–210. [[CrossRef](#)]
15. Doutsos, T.; Piper, D.J. Listric faulting, sedimentation, and morphological evolution of the Quaternary eastern Corinth rift, Greece: First stages of continental rifting. *GSA Bull.* **1990**, *102*, 812–829. [[CrossRef](#)]
16. Armijo, R.; Meyer, B.; King, G.C.P.; Rigo, A.; Papanastassiou, D. Quaternary evolution of the Corinth Rift and its implications for the Late Cenozoic evolution of the Aegean. *Geophys. J. Int.* **1996**, *126*, 11–53. [[CrossRef](#)]
17. Sorel, D. A Pleistocene and still-active detachment fault and the origin of the Corinth–Patras rift (Greece). *Geology* **2000**, *28*, 83–86. [[CrossRef](#)]
18. Collier, R.; Jones, G. Rift Sequences of the Southern Margin of the Gulf of Corinth (Greece) as Exploration/Production Analogues. In Proceedings of the American Association of Petroleum Geologists International Conference, Search and Discovery Article no. 90017, Barcelona, Spain, 21–24 September 2003.
19. Ford, M.; Rohais, S.; Williams, E.A.; Bourlange, S.; Joussetin, D.; Backert, N.; Malartre, F. Tectono-sedimentary evolution of the western Corinth rift (Central Greece). *Basin Res.* **2012**, *25*, 3–25. [[CrossRef](#)]
20. Ford, M.; Hemelsdael, R.; Mancini, M.; Palyvos, N. Rift migration and lateral propagation: Evolution of normal faults and sediment-routing systems of the western Corinth rift (Greece). In *The Geometry of Normal Faults*; Childs, C., Holdsworth, R.E., Jackson, C.A., Manzocchi, T., Walsh, J.J., Yielding, G., Eds.; Geological Society, Special Publications: London, UK, 2016.
21. Pirazzoli, P.; Stiros, S.; Fontugne, M.; Arnold, M. Holocene and Quaternary uplift in the central part of the southern coast of the Corinth Gulf (Greece). *Mar. Geol.* **2004**, *212*, 35–44. [[CrossRef](#)]
22. Billiris, H.; Paradissis, D.; Veis, G.; England, P.; Featherstone, W.; Parsons, B.; Cross, P.; Rands, P.; Rayson, M.; Sellers, P.; et al. Geodetic determination of tectonic deformation in central Greece from 1900 to Nat. *Cell Biol.* **1991**, *350*, 124–129. [[CrossRef](#)]
23. Davies, R.; England, P.; Parsons, B.; Billiris, H.; Paradissis, D.; Veis, G. Geodetic strain of Greece in the interval 1892–1992. *J. Geophys. Res. Space Phys.* **1997**, *102*, 24571–24588. [[CrossRef](#)]
24. Briole, P.; Rigo, A.; Lyon-Caen, H.; Ruegg, J.; Papazissi, K.; Mistakaki, C.; Balodimou, A.; Veis, G.; Hatzfeld, D.; Deschamps, A. Active deformation of the gulf of Korinthos, Greece: Results from repeated GPS surveys between 1990 and 1995. *JGR* **2000**, *105*, 25605–25625. [[CrossRef](#)]
25. Palyvos, N.; Mancini, M.; Sorel, D.; Lemeille, F.; Pantosti, D.; Julia, R.; Triantaphyllou, M.; De Martini, P.-M. Geomorphological, stratigraphic and geochronological evidence of fast Pleistocene coastal uplift in the westernmost part of the Corinth Gulf Rift (Greece). *Geol. J.* **2009**, *45*, 78–104. [[CrossRef](#)]
26. Jackson, J.; Gagnepain, J.; Houseman, G.; King, G.; Papadimitriou, P.; Soufleris, C.; Virieux, J. Seismicity, normal faulting, and the geomorphological development of the Gulf of Corinth (Greece): The Corinth earthquakes of February and March Earth Planet. *Sci. Lett.* **1982**, *57*, 377–397. [[CrossRef](#)]

27. King, G.C.P.; Ouyang, Z.X.; Papadimitriou, P.; Deschamps, A.; Gagnepain, J.; Houseman, G.; Jackson, J.A.; Soufleris, C.; Virieux, J. The evolution of the Gulf of Corinth (Greece): An aftershock study of the 1981 earthquakes. *Geophys. J. Int.* **1985**, *80*, 677–693. [[CrossRef](#)]
28. Pavlides, S. Active faulting in multi-fractured seismogenic areas; examples from Greece. *Z. Geomorphol. Suppl.* **1993**, *94*, 57–72.
29. Tselentis, A.; Melis, N.; Sokos, E.; Papatsimpa, K. The Egion June 15, 1995 (6.2 ML) earthquake, Western Greece. *Pure Appl. Geophys.* **1996**, *147*, 83–98. [[CrossRef](#)]
30. Koukouvelas, I.; Doutsos, T. Implications of structural segmentation during earthquakes: The 1995 Egion earthquake, Gulf of Corinth, Greece. *J. Struct. Geol.* **1996**, *18*, 1381–1388. [[CrossRef](#)]
31. Bernard, P.; Lyon Caen, H.; Briole, P.; Deschamps, A.; Boudin, F.; Makropoulos, K.; Papadimitriou, P.; Lemeille, F.; Patau, G.; Billiris, H.; et al. Seismicity, deformation and seismic hazard in the western rift of Corinth: New insights from the Corinth Rift Laboratory (CRL). *Tectonophysics* **2006**, *426*, 7–30. [[CrossRef](#)]
32. Karakostas, V.; Karagianni, E.; Paradisopoulou, P. Space–time analysis, faulting and triggering of the 2010 earthquake doublet in western Corinth Gulf. *Nat. Hazards* **2012**, *63*, 1181–1202. [[CrossRef](#)]
33. Doutsos, T.; Koukouvelas, I.K.; Xypolias, P. A new orogenic model for the External Hellenides. *Geol. Soc. Spec. Publ.* **2006**, *260*, 507–520. [[CrossRef](#)]
34. Doutsos, T.; Kontopoulos, N.; Poulimenos, G. The Corinth-Patras rift as the initial stage of continental fragmentation behind an active island arc (Greece). *Basin Res.* **2007**, *1*, 177–190. [[CrossRef](#)]
35. Piper, D.J.W.; Kontopoulos, N.; Anagnostou, C.; Chronis, G.; Panagos, A.G. Modern fan deltas in the western Gulf of Corinth, Greece. *Geo-Marine Lett.* **1990**, *10*, 5–12. [[CrossRef](#)]
36. Poulimenos, G.; Zelilidis, A.; Kontopoulos, N.; Doutsos, T. Geometry of trapezoidal fan deltas and their relationship to extensional faulting along the southwestern active margins of the Corinth rift, Greece. *Basin Res.* **1993**, *5*, 179–192. [[CrossRef](#)]
37. Zelilidis, A. Drainage evolution in a rifted basin, Corinth graben, Greece. *Geomorphology* **2000**, *35*, 69–85. [[CrossRef](#)]
38. Zelilidis, A. The geometry of fan-deltas and related turbidites in narrow linear basins. *Geol. J.* **2003**, *38*, 31–46. [[CrossRef](#)]
39. Rohais, S.; Eschard, R.; Guillocheau, F. Depositional model and stratigraphic architecture of rift climax Gilbert-type fan deltas (Gulf of Corinth, Greece). *Sediment. Geol.* **2008**, *210*, 132–145. [[CrossRef](#)]
40. Papatheodorou, G.; Stefatos, A.; Christodoulou, D.; Ferentinos, G. Small Scale Present Day Turbidity Currents in a Tectonically Active Submarine Graben, The Gulf of Corinth (Greece): Their Significance in Dispersing Mine Tailings and Their Relevance to Basin Filling. In *Drought and Drought Mitigation in Europe*; Springer: Berlin/Heidelberg, Germany, 2003; Volume 19, pp. 459–468.
41. Moretti, I.; Lykousis, V.; Sakellariou, D.; Reynaud, J.-Y.; Benziane, B.; Prinzhofer, A. Sedimentation and subsidence rate in the Gulf of Corinth: What we learn from the Marion Dufresne’s long-piston coring. *Comptes Rendus Geosci.* **2004**, *336*, 291–299. [[CrossRef](#)]
42. Lykousis, V.; Sakellariou, D.; Moretti, I.; Kaberi, H. Late Quaternary basin evolution of the Gulf of Corinth: Sequence stratigraphy, sedimentation, fault-slip and subsidence rates. *Tectonophysics* **2007**, *440*, 29–51. [[CrossRef](#)]
43. Beckers, A.; Hubert-Ferrari, A.; Beck, C.; Papatheodorou, G.; de Batist, M.; Sakellariou, D.; Tripsanas, E.; Demoulin, A. Characteristics and frequency of large submarine landslides at the western tip of the Gulf of Corinth. *Nat. Hazards Earth Syst. Sci.* **2017**, *18*, 1411–1425. [[CrossRef](#)]
44. De Martini, P.M.; Pantosti, D.; Palyvos, N.; Lemeille, F.; McNeill, L.; Collier, R. Slip rates of the Aigion and Eliki Faults from uplifted marine terraces, Corinth Gulf, Greece. *Comptes Rendus Geosci.* **2004**, *336*, 325–334. [[CrossRef](#)]
45. Karymbalis, E.; Chalkias, C.; Chalkias, G.; Grigoropoulou, E.; Manthos, G.; Ferentinou, M. Assessment of the sensitivity of the southern coast of the Gulf of Corinth (Peloponnese, Greece) to sea-level rise. *Open Geosci.* **2012**, *4*, 561–577. [[CrossRef](#)]
46. Hemelsdaël, R.; Malartre, F.; Gawthorpe, R.; Ford, M. Interaction of an antecedent fluvial system with early normal fault growth: Implications for syn-rift stratigraphy, western Corinth rift (Greece). *Sedimentology* **2017**, *64*, 1957–1997. [[CrossRef](#)]
47. Hatzfeld, D.; Karakostas, V.; Ziazia, M.; Kassaras, I.; Papadimitriou, E.; Makropoulos, K.; Voulgaris, N.; Papaioannou, C. Microseismicity and faulting geometry in the Gulf of Corinth (Greece). *Geophys. J. Int.* **2000**, *141*, 438–456. [[CrossRef](#)]
48. Sachpazi, M.; Clément, C.; Laigle, M.; Hirn, A.; Roussos, N. Rift structure, evolution, and earthquakes in the Gulf of Corinth, from reflection seismic images. *Earth Planet. Sci. Lett.* **2003**, *216*, 243–257. [[CrossRef](#)]
49. Cowie, P.; Gupta, S.; Dawers, N. Implications of fault array evolution for synrift depocentre development: Insights from a numerical fault growth model. *Basin Res.* **2000**, *12*, 241–261. [[CrossRef](#)]
50. Stefatos, A.; Papatheodorou, G.; Ferentinos, G.; Leeder, M.; Collier, R. Seismic reflection imaging of active offshore faults in the Gulf of Corinth: Their seismotectonic significance. *Basin Res.* **2002**, *14*, 487–502. [[CrossRef](#)]
51. Taylor, B.; Weiss, J.R.; Goodliffe, A.M.; Sachpazi, M.; Laigle, M.; Hirn, A. The structures, stratigraphy and evolution of the Gulf of Corinth rift, Greece. *Geophys. J. Int.* **2011**, *185*, 1189–1219. [[CrossRef](#)]
52. Gawthorpe, R.L.; Leeder, M.R.; Kranis, H.; Skourtsos, E.; Andrews, J.E.; Henstra, G.A.; Mack, G.H.; Muravchik, M.; Turner, J.A.; Stamatakis, M. Tectono-sedimentary evolution of the Plio-Pleistocene Corinth rift, Greece. *Basin Res.* **2018**, *30*, 448–479. [[CrossRef](#)]
53. Collier, R.E.L.; Leeder, M.R.; Trout, M.; Ferentinos, G.; Lyberis, E.; Papatheodorou, G. High sediment yields and cool, wet winters: Test of last glacial paleoclimates in the northern Mediterranean. *Geology* **2000**, *28*, 999–1002. [[CrossRef](#)]
54. Finnegan, N.J.; Hallet, B.; Montgomery, D.R.; Zeitler, P.K.; Stone, J.O.; Anders, A.; Yuping, L. Coupling of rock uplift and river incision in the Namche Barwa-Gyala Peri massif, Tibet. *GSA Bull.* **2008**, *120*, 142–155. [[CrossRef](#)]
55. Kirby, E.; Whipple, K.X. Expression of active tectonics in erosional landscapes. *J. Struct. Geol.* **2012**, *44*, 54–75. [[CrossRef](#)]

56. Koukouvelas, I.K. Transfer zones along active normal faults in Peloponnesus, Greece. *Bull. Geol. Soc. Greece* **1998**, *32*, 221–229.
57. Ganas, A.; Pavlides, S.; Karastathis, V. DEM-based morphometry of range-front escarpments in Attica, central Greece, and its relation to fault slip rates. *Geomorphology* **2005**, *65*, 301–319. [[CrossRef](#)]
58. Zygouri, V.; Koukouvelas, I.K.; Kokkalas, S.; Xypolias, P.; Papadopoulos, G.A. The Nisi Fault as a Key structure for understanding the active deformation of the NW Peloponnese, Greece. *Geomorphology* **2015**, *237*, 142e156. [[CrossRef](#)]
59. Koukouvelas, I.K.; Zygouri, V.; Verroios, S.; Nikolakopoulos, K. Treatise on the tectonic geomorphology of active faults: The significance of using a universal digital elevation model. *J. Struct. Geol.* **2018**, *116*, 241–252. [[CrossRef](#)]
60. Roberts, S.; Jackson, J. Active normal faulting in central Greece: An overview. *Geol. Soc. Spec. Publ. Lond.* **1991**, *56*, 125–142.
61. Pavlides, S.; Koukouvelas, I.; Kokkalas, S.; Stamatopoulos, L.; Keramydas, D.; Tsodoulos, I. Late Holocene evolution of the East Eliki fault, Gulf of Corinth (Central Greece). *Quat. Int.* **2004**, *115–116*, 139–154. [[CrossRef](#)]
62. Tsodoulos, I.M.; Koukouvelas, I.K.; Pavlides, S. Tectonic geomorphology of the easternmost extension of the Gulf of Corinth (Beotia, Central Greece). *Tectonophysics* **2008**, *453*, 211–232. [[CrossRef](#)]
63. Karalis, S.; Karymbalis, E.; Valkanou, K.; Chalkias, C.; Katsafados, P.; Kalogeropoulos, K.; Batzakis, V.; Bofilios, A. Assessment of the relationships among catchments' morphometric parameters and hydrologic indices. *Int. J. Geosci.* **2014**, *5*, 1571–1583.
64. McClusky, S.; Balassanian, S.; Barka, A.; Demir, C.; Ergintav, S.; Georgiev, I.; Gurkan, O.; Hamburger, M.; Hurst, K.; Kahle, H.; et al. Global Positioning System constraints on plate kinematics and dynamics in the eastern Mediterranean and Caucasus. *J. Geophys. Res.* **2000**, *105*, 5695–5719. [[CrossRef](#)]
65. Taymaz, T.; Jackson, J.; McKenzie, D. Active tectonics of the north and central Aegean Sea. *Geophys. J. Int.* **1991**, *106*, 433–490. [[CrossRef](#)]
66. Doutsos, T.; Kokkalas, S. Stress and deformation patterns in the Aegean region. *J. Struct. Geol.* **2001**, *23*, 455–472. [[CrossRef](#)]
67. Papazachos, B.C.; Comninakis, P.E.; Karakaisis, G.F.; Karakostas, B.G.; Papaioannou, C.A.; Papazachos, C.B.; Scordilis, E.M. *A Catalogue of Earthquakes in Greece and Surrounding Area for the Period 1901–1999*; Geophysical Laboratory, Aristotle University of Thessaloniki: Thessaloniki, Greece, 2000.
68. Tiberi, C.; Diament, M.; Lyon-Caen, H.; King, T. Moho topography beneath the Corinth Rift area (Greece) from inversion of gravity data. *Geophys. J. Int.* **2001**, *145*, 797–808. [[CrossRef](#)]
69. Nyst, M.; Thatcher, W. New constraints on the active tectonic deformation of the Aegean. *J. Geophys. Res. Space Phys.* **2004**, *109*, 11406. [[CrossRef](#)]
70. Papanikolaou, D.; Royden, L.H. Disruption of the Hellenic arc: Late Miocene extensional detachment faults and steep Plio-cene-Quaternary normal faults—Or what happened at Corinth? *Tectonics* **2007**, *26*. [[CrossRef](#)]
71. Charalampakis, M.; Stefanos, A.; Hasiotis, T.; Ferentinos, G. Submarine Mass Movements On An Active Fault System In The Central Gulf Of Corinth. In *Submarine Mass Movements and Their Consequences*; Springer: Berlin/Heidelberg, Germany, 2007; pp. 67–75.
72. Cullen, T.M.; Collier, R.E.L.; Gawthorpe, R.L.; Hodgson, D.M.; Barrett, B.J. Axial and transverse deep-water sediment supply to syn-rift fault terraces: Insights from the West Xylokastro Fault Block, Gulf of Corinth, Greece. *Basin Res.* **2020**, *32*, 1105–1139. [[CrossRef](#)]
73. Place, J.; Géraud, Y.; Diraison, M.; Warr, L. North–south transfer zones and paleo–morphological reconstruction of the Xylocastro area (Corinth Gulf, Greece). *Tectonophysics* **2007**, *440*, 121–139. [[CrossRef](#)]
74. Skourtsos, E.; Kranis, H. Structure and evolution of the western Corinth Rift, through new field data from the Northern Peloponnesus. In *Extending a Continent: Architecture, Rheology and Heat Budget*; Ring, U., Wernicke, B., Eds.; Geological Society of London, Special Publication: London, UK, 2009; Volume 321, pp. 119–138.
75. Rohais, S.; Moretti, I. Structural and stratigraphic architecture of the Corinth Rift (Greece): An integrated onshore to offshore basin-scale synthesis. In *Lithosphere Dynamics and Sedimentary Basins of the Arabian Plate and Surrounding Areas*; Roure, F., Amin, A.A., Khoms, S., Al Garni, M.A.M., Eds.; Cham Springer International Publishing: Copenhagen, Denmark, 2017; pp. 89–120.
76. Keller, E.A.; Pinter, N. *Active Tectonics: Earthquakes, Uplift and Landscape*; Prentice Hall: Hoboken, NJ, USA, 1996.
77. Delcaillau, B. *Reliefs et Tectonique Recente Nouveau Précis de Géomorphologie*; Paris, France. 2004, p. 262. Available online: <https://hal.archives-ouvertes.fr/hal-01896068/> (accessed on 20 November 2021).
78. Singh, P.; Thakur, J.K.; Singh, U.C. Morphometric analysis of Morar River Basin, Madhya Pradesh, India, using remote sensing and GIS techniques. *Environ. Earth Sci.* **2012**, *68*, 1967–1977. [[CrossRef](#)]
79. Dar, R.A.; Romshoo, S.; Chandra, R.; Ahmad, I. Tectono-geomorphic study of the Karewa Basin of Kashmir Valley. *J. Asian Earth Sci.* **2014**, *92*, 143–156. [[CrossRef](#)]
80. Koukouvelas, I.; Stamatopoulos, L.; Katsonopoulou, D.; Pavlides, S. A paleoseismological and geoarchaeological investigation of Eliki fault, Gulf of Corinth, Greece. *J. Struct. Geol.* **2001**, *23*, 531–543. [[CrossRef](#)]
81. Quesada-Román, A.; Campos, N.; Alcalá-Reygosa, J.; Granados-Bolaños, S. Equilibrium-line altitude and temperature reconstructions during the Last Glacial Maximum in Chirripó National Park, Costa Rica. *J. S. Am. Earth Sci.* **2020**, *100*, 102576. [[CrossRef](#)]
82. Quesada-Román, A.; Campos, N.; Granados-Bolaños, S. Tropical glacier reconstructions during the Last Glacial Maximum in Costa Rica. *Rev. Mex. Cienc. Geol.* **2021**, *38*, 55–64. [[CrossRef](#)]
83. Quesada-Román, A.; Vargas-Sanabria, D. A geomorphometric model to determine topographic parameters controlling wildfires occurrence in tropical dry forests. *J. Arid. Environ.* **2021**, *198*, 104674. [[CrossRef](#)]

84. Koukouvelas, I.K.; Zygouri, V.; Papadopoulos, G.A.; Verroios, S. Holocene record of slip-predictable earthquakes on the Kenchreai Fault, Gulf of Corinth, Greece. *J. Struct. Geol.* **2017**, *94*, 258–274.
85. Philips, L.F.; Schumm, S.A. Effect of regional slope on drainage networks. *Geology* **1987**, *15*, 813–816. [[CrossRef](#)]
86. Cox, R.T. Analysis of drainage-basin symmetry as a rapid technique to identify areas of possible Quaternary tilt-block tectonics: An example from the Mississippi Embayment. *Geol. Soc. Am. Bull.* **1994**, *106*, 571–581. [[CrossRef](#)]
87. Hack, J. Stream profile analysis and stream gradient index. *U.S. Geol. Surv. J. Res. Explor. Athens* **1973**, *1*, 421–429.
88. Bull, W.B.; McFadden, L.D. Tectonic Geomorphology North and South of the Garlock Fault, California. In *Geomorphology in Arid regions*; Doehring, D.O., Ed.; State University of New York: Binghamton, NY, USA, 1977; pp. 115–138.
89. El Hamdouni, R.; Irigaray, C.; Fernández, T.; Chacón, J.; Keller, E. Assessment of relative active tectonics, southwest border of the Sierra Nevada (southern Spain). *Geomorphology* **2008**, *96*, 150–173. [[CrossRef](#)]
90. Azor, A.; Keller, E.A.; Yeats, R.S. Geomorphic indicators of active fold growth: Oak Ridge anticline, Ventura basin, southern California. *GSA Bull.* **2002**, *114*, 745–753. [[CrossRef](#)]
91. Verrios, S.; Zygouri, V.; Kokkalas, S. Morphotectonic Analysis in the Eliki Fault Zone (Gulf of Corinth, Greece). *Bull. Geol. Soc. Greece* **2004**, *36*, 1706–1715. [[CrossRef](#)]
92. Silva, P.G.; Goy, J.; Zazo, C.; Bardají, T. Fault-generated mountain fronts in southeast Spain: Geomorphologic assessment of tectonic and seismic activity. *Geomorphology* **2003**, *50*, 203–225. [[CrossRef](#)]
93. Rockwell, T.; Keller, E.; Johnson, D. Tectonic geomorphology of alluvial fans and mountain fronts near Ventura, California. In *Tectonic Geomorphology*; Morisawa, M., Hack, T.J., Eds.; State University of New York: Binghamton, NY, USA, 1985; pp. 183–207.
94. Demoulin, A.; Beckers, A.; Hubert-Ferrari, A. Patterns of Quaternary uplift of the Corinth rift southern border (N Peloponnese, Greece) revealed by fluvial landscape morphometry. *Geomorphology* **2015**, *246*, 188–204. [[CrossRef](#)]